## PROCEEDINGS OF SPIE

SPIEDigitalLibrary.org/conference-proceedings-of-spie

# High-speed nano-polarimetry for real-time plasmonic bio-imaging

Yipei Wang, Yunbo Liu, Xintao Zhao, Somin Eunice Lee

Yipei Wang, Yunbo Liu, Xintao Zhao, Somin Eunice Lee, "High-speed nano-polarimetry for real-time plasmonic bio-imaging," Proc. SPIE 10509, Plasmonics in Biology and Medicine XV, 1050908 (23 February 2018); doi: 10.1117/12.2289144



Event: SPIE BiOS, 2018, San Francisco, California, United States

### High-speed nano-polarimetry for real-time plasmonic bio-imaging

Yipei Wang, Yunbo Liu, Xintao Zhao, Somin Eunice Lee\*

Department of Electrical & Computer Engineering, University of Michigan, Ann Arbor, MI 48109,

Department of Biomedical Engineering, University of Michigan, Ann Arbor, MI 48109,

Biointerfaces Institute, University of Michigan, Ann Arbor, MI 48109,

#### **ABSTRACT**

Plasmonic nanoparticles are excellent nonbleaching probes for bio-imaging. Due to their anisotropic properties, polarization analysis of individual nanoparticles allows for revealing orientational information, plasmon mode assignment, and the local microenvironment. Previous implementations utilize mechanical rotation of conventional polarizers to align the polarization angles with specific axes of nanoparticles. However, the manufacturing defects of the polarizer (e.g., non-parallelism) limit the measurement stability (e.g., beam wobbling) in polarimetric imaging, while the mechanical rotation limits the measurement speed, and thus hinders accurate, real-time acquisition of individual nanoparticles.

Here, we demonstrate a high-speed nano-polarimetric system for stable plasmonic bio-imaging by integrating our voltage-tunable polarizer (VTP) into a microscope. The angular rotation of the polarization  $(0 \sim \pi)$  can be realized by applying voltage on the VTP. We show that our voltage-tunable system offers high extinction ratio ( $\sim$ up to 250), and uniform transmission ( $\sim$ 55%) over a large input power range (<5% deviation for input power from 50  $\mu$ W to  $\sim$ 20 mW). Meanwhile, the transmission polarization can be rapidly tuned with a response time up to 50 ms. Compared to conventional polarizers, our system is able to provide reproducible and high-speed polarimetric images of individual nanoparticles with sub-pixel spatial precision. Such a polarimetric nanoimaging system could be a useful tool for real-time single nanoparticle bio-imaging with both high stability and time resolution.

Keywords: plasmonic nanoparticle, bio-imaging, high speed, spatial stability

#### 1. INTRODUCTION

Owing to their unique properties, including large scattering cross-section and excellent photo-stability, plasmonic nanoparticles have been attracting considerable attention for bio-imaging. By rotating the polarization to align with the axes of anisotropic nanoparticles, 1.2 polarimetric imaging of individual nanoparticles further allows for resolving spatial information and the local bio-environment. 3-5 Ideally, it would be desirable in many biomedical applications to ascertain the spatial position of individual plasmonic nanoparticle (*e.g.*, nanometer) with both high spatial stability and fast polarization tuning speed. For example, in polarimetry-based single particle tracking, imaging stability and polarization rotation speed directly determine the localization precision and temporal resolution (Figure 1). In previous implementations, a mechanically rotated polarizer is usually placed in the detection paths before the CCD. 6-8 However, the manufacturing defects (*e.g.*, non-parallelism of the polarizer, wobbling of the rotary mount) limit the imaging stability (*e.g.*, beam deviation), while the mechanical rotation limits the imaging speed. In this paper, we present a high-speed nano-polarimetric system for stable plasmonic nano-imaging. By integrating our voltage-tunable polarizer (VTP) into a dark-field microscope, voltage rather than mechanical rotation is used to rapidly tune the transmission polarization angles. Compared to a conventional mechanical setup which is prone to beam deviation errors, our nano-imaging system is able to offer spatially stable, reproducible polarimetric nano-images, allowing for high-speed, real-time acquisition of individual plasmonic nanoparticles without image correction.

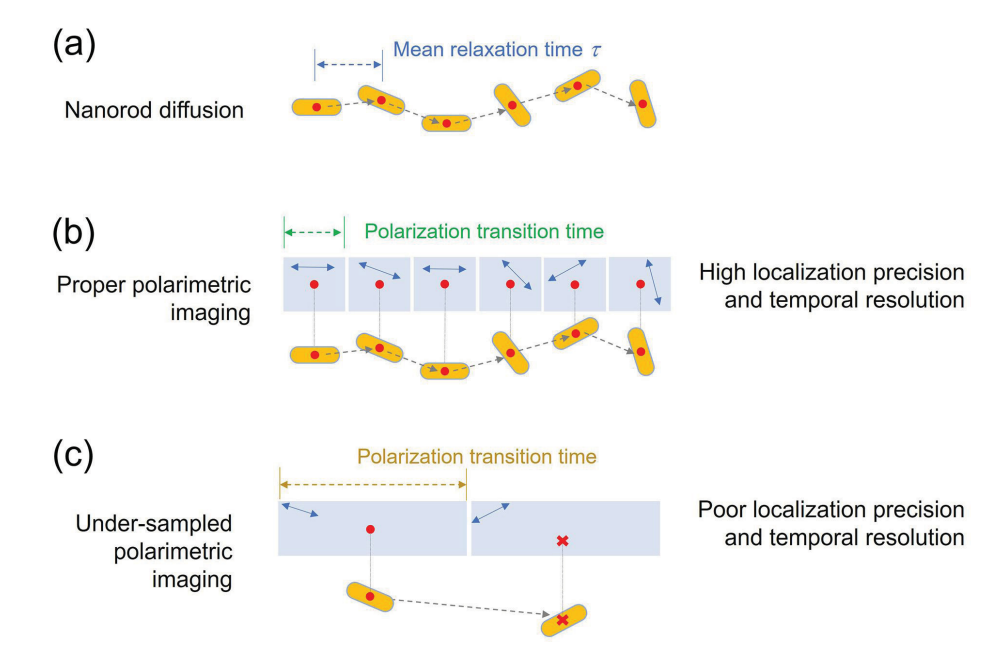


Figure 1. High localization precision and temporal resolution are desirable in polarimetric imaging. (a) Polarimetric imaging in bio-applications: As a typical case, single-nanoparticle tracking is a useful tool for probing the microenvironment in biological applications. For individual nanorods, the diffusion exhibits both translational (gray dashed-arrow) and rotational motions with a mean relaxation time ( $\tau$ , time interval between different orientations, blue double-headed arrow) at the ms level. (b) **Proper polarimetric imaging**: Polarimetric imaging with sufficient localization precision and temporal resolution, reveals the true trajectory and rotational dynamics of nanorods. Blue block represents the time scale of intervals between each polarization rotation. The response time of polarization rotation (green double-headed arrow) should be less than the mean relaxation time  $\tau$ . Blue double-headed arrow indicates the polarization direction for imaging. (c) **Under-sampled polarimetric imaging**: Insufficient localization precision and temporal resolution hinder resolving the nanorod trajectory and rotations. Blue block represents the time scale of intervals between each polarization rotation. If the response time (gold double-headed arrow) is longer than the mean relaxation time, then the rotational dynamics cannot be fully resolved. Meanwhile, if the polarization rotation introduces beam deviations (red cross), then the spatial position of nanorod cannot be correctly determined.

#### 2. THEORY

The angular rotation  $(\theta)$  of a polarizer can be treated as operating the Mueller matrices on the Stokes vector of the input light  $[I_i, Q_i, U_i, V_i]^{T.9}$  For the CCD detector, the intensity  $I(\theta)$  can be expressed as

$$I(\theta) = \frac{1}{2} (I_i + Q_i \cos 2\theta + U_i \sin 2\theta). \tag{1}$$

Meanwhile, for imaging nanoparticles, the intensity on the CCD takes the form of a Gaussian distribution, in which Eq. (1) can be rewritten as

$$I(x, y; \theta) = \frac{1}{2} \left( I_i + Q_i \cos 2\theta + U_i \sin 2\theta \right) \exp\left[ -2 \frac{(x - x_\theta)^2 + (y - y_\theta)^2}{\omega^2} \right], \tag{2}$$

where  $(x_{\theta}, y_{\theta})$  is the coordinate of the beam center with respect to the rotation angle  $(\theta)$ , and the  $\omega$  is the waist radius. In the experimental case, the actual output signal  $S(m, n; \theta)$  from a CCD pixel (m, n) can be then given by  $S(m, n; \theta)$ 

$$S(m, n; \theta) = \frac{1}{2} \int_{-\infty}^{+\infty} \int_{-\infty}^{+\infty} \left( I_i + Q_i \cos 2\theta + U_i \sin 2\theta \right) \exp\left[ -2 \frac{(x - x_\theta)^2 + (y - y_\theta)^2}{\omega^2} \right] R(x - mp, y - nq) dx dy, \quad (3)$$

where R(x, y) is the pixel response function (PRF), and p, q is the pixel pitch in the x and y directions, respectively. Ideally, the beam center  $(x_{\theta}, y_{\theta})$  should remain at the same position regardless of the rotation of the polarizer (Figure 2(a)-i). However, in the experiment case, beam deviation caused by the rotation is inevitable due to mechanical and manufacturing limitations, including the wobble of the polarizer rotation mount and the non-parallelism of the polarizer (Figure 2(a)-ii). For quantitively characterization, the beam deviation ( $\Delta l$ ) is defined as

$$\Delta l = \sqrt{(x_{\theta} - x_0)^2 + (y_{\theta} - y_0)^2},$$
(4)

where  $(x_0, y_0)$  is the coordinate of the beam center before the rotation of the polarizer. By applying basic geometric optics, the maximum beam deviation caused by the mount wobbling can be obtained as

$$\Delta l \approx d_1 \frac{n-1}{n} \sigma_1,\tag{5}$$

where  $d_1$  is the thickness of the mounted polarizer,  $\sigma_1$  is the maximum wobble angle, and n is the refractive index of the polarizer (typically ~1.45). Typically,  $d_1$  (~several millimeter) and  $\sigma_1$  (~µrad level) are relatively small, resulting a negligible  $\Delta l$  (at the nanometer scale) compared to the size of the pixel in the CCD detector (at the sub-micrometer scale). On the other hand, the beam deviation due to the non-parallelism of a polarizer can be obtained as

$$\begin{cases} x_{\theta} = d_2 \, \sigma_2(n-1)(1-\cos\theta) \\ y_{\theta} = d_2 \sigma_2(n-1)\sin\theta \\ \Delta l(\theta) = 2\sin(\theta/2)d_2(n-1)\sigma_2 \end{cases}$$
(6)

where  $d_2$  is the distance between the CCD and the polarizer (typically ~50 mm), and  $\sigma_2$  is the non-parallel angle between the two optical surfaces of the polarizer (typically ~5 arcsec). By taking the typical values into Eq. (6), the calculated beam deviation caused by the rotation of the polarizer is as large as ~1.1 µm at the imaging plane. More importantly, such beam deviation gives rise to a significant intensity error at the imaging plane, which cannot be fully corrected by image processing. For better understanding, by combining the Eq. (6) and Eq. (3), polarimetric images using a non-parallelism polarizer can be calculated as

$$S(m,n;\theta) = \frac{1}{2} \left( I_s + Q_s \cos 2\theta + U_s \sin 2\theta \right)$$

$$\int_{-\infty}^{+\infty} \int_{-\infty}^{+\infty} \exp \left\{ -2 \frac{\left[ x - d_2 \sigma_2(n-1)(1 - \cos \theta) \right]^2 + \left[ y - d_2 \sigma_2(n-1)\sin \theta \right]^2}{\omega^2} \right\} R(x - mp, y - nq) dx dy.$$
(7)

The CCD was assumed to have an ideal PRF R(x, y) with the constant value of 1 inside the pixel. The pixel size was set to be 250 nm × 250 nm. The waist radius of the gaussian distribution was assumed to be 500 nm. As a typical case in bio-imaging, a nanorod with the orientation aligned with the x-axis was selected for simulation. The resulting Stokes vector of the nanorod was set to be  $[1,1,0,0]^T$ . Figure 2(b) shows the calculated plasmonic nano-imaging with an ideal polarizer (Figure 2(b)-i) and a mechanically rotated polarizer (Figure 2(b)-ii). It can be seen that the spatial instability at the micrometer scale arises from the non-parallelism of the mechanically rotated polarizer. Moreover, even with an ideal PRF, the beam deviation at the sub-pixel scale changes the intensity distribution in the spatial domain due to the sampling of the CCD, giving rise to an uncorrectable intensity error for each pixel (Figure 2(b)-iii).

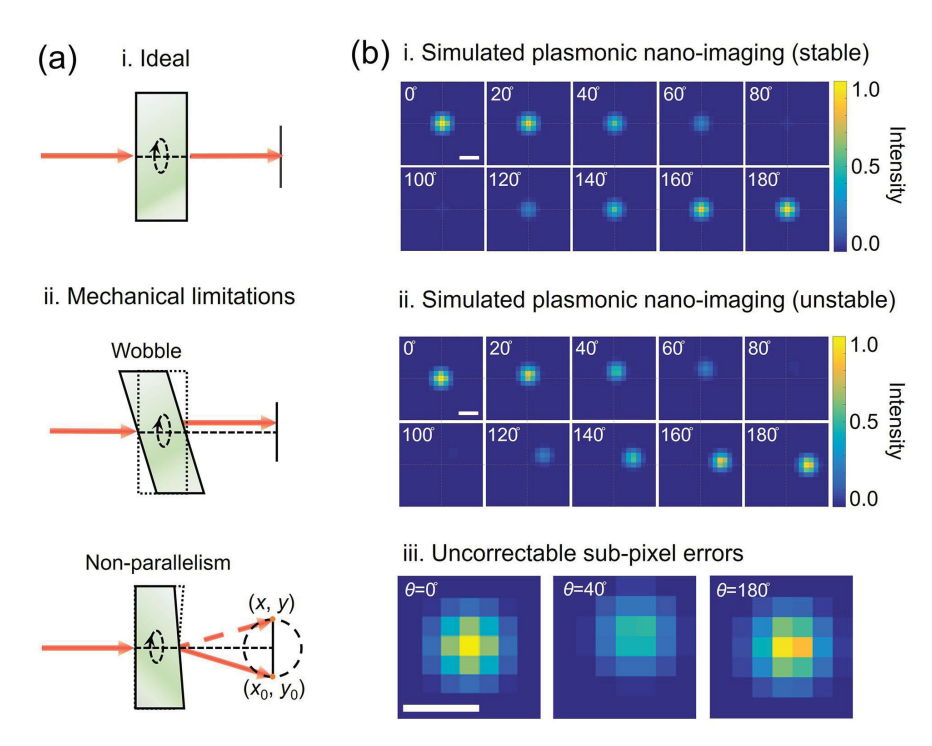


Figure 2. Beam deviation and spatial instability arise from mechanical and manufacturing limitations. (a) Beam deviation: (i) Ideal case. (ii) Mechanical limitations including wobbling and non-parallelism. (b) Simulated plasmonic nano-imaging: (i) Stable polarimetric nano-images of a single plasmonic nanorod in the ideal case. (ii) Unstable polarimetric nano-images of a single plasmonic nanorod arise using a mechanically rotated polarizer and show significant beam deviation at the micrometer scale. (iii) Close-up views ( $\theta$ =0, 40 and 180) showing uncorrectable beam deviation errors at the sub-pixel scale. The scale bars are 1  $\mu$ m.

#### 3. POLARIMETRIC IMAGING SETUP

Our nano-imaging system (Figure 3) consisted a dark-field microscope configured with a halogen light source, an adjustable diaphragm, a dry condenser, a 50x objective, a CCD camera, and our voltage-tunable polarizer (VTP). The VTP consisted of liquid crystal retarders (refer to LCA and LCB) and waveplates. The tuning of the transmission polarization was realized by applying different voltages on the liquid crystal retarders through a two-channel function generator. The actuation voltage and the image acquired from the CCD were automated to realize high-speed imaging with integration time at the ms level. To achieve high-quality nanoimaging, the optical elements and the diaphragm were carefully aligned and adjusted for proper Kohler illumination.

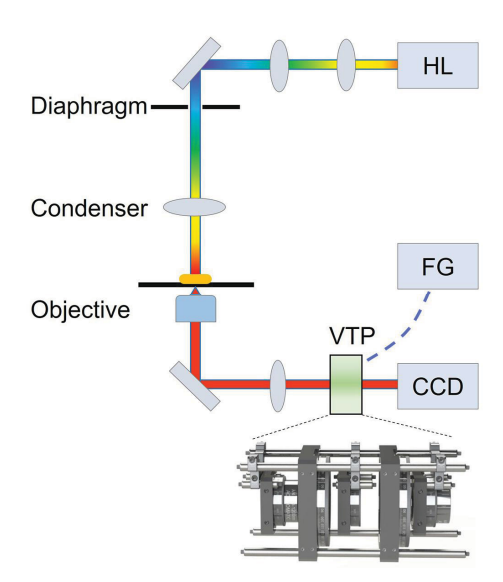


Figure 3. Schematics of high-speed, stable nano-imaging enabled by voltage-tunable polarizer (VTP). The polarimetric nano-imaging system integrates the output of a dark-field microscope with a VTP composed of waveplates and liquid crystal retarders. HL: halogen light sources. FG: function generator.

#### 4. RESULTS AND DISCUSSION

To achieve the optimum performance for plasmonic nano-imaging, we first systematically characterized the VTP in terms of actuation voltages, extinction ratio, and power dependence (Figure 4). For characterization (Figure 4(a) inset), a Ti:Sapphire CW laser with a wavelength of 720 nm was used as the light source. The laser beam was split into two beams by a 50:50 beam splitter. One of the beams was directed to a power meter for real-time measurement of the input intensity ( $P_1$ ). The other beam was directed through a commercial linear polarizer and our VTP, and was collected by another power meter to measure the output intensity ( $P_2$ ). The transmission of the VTP can then be obtained by  $P_2/P_1$ .

Actuation voltages for tuning the transmission polarization axis ( $\theta$ ) exhibited excellent linearity within the polarization angles from 0° to 180° shown in Figure 4(a). When the applied voltages to the liquid crystal retarders increased, the intensity of the transmitted light varied from minimum to maximum, and then decreased to a minimum with an extinction ratio of ~250. Note that the polarization-dependent intensity fits well to a sinusoidal function, showing an excellent match to Malus's law. In addition, for given angles of the transmission polarization axis (e.g., 0°, red line), the voltage-tunable polarizer exhibited a uniform transmission (~52%) over a large input power range (from 50  $\mu$ W to 16 mW) with deviations less than 5%.

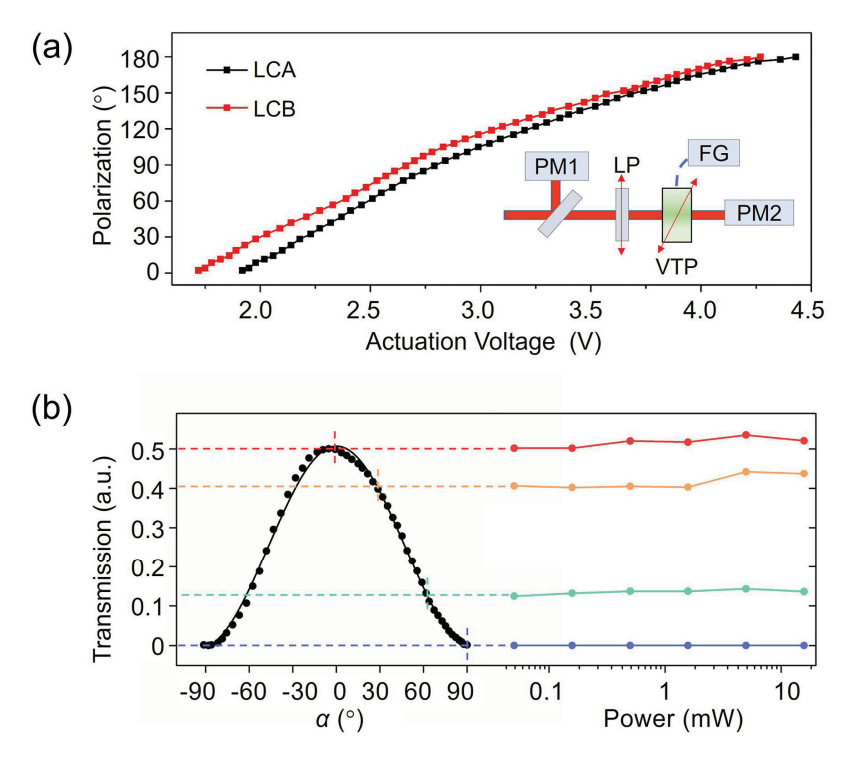


Figure 4. The voltage-tunable polarizer (VTP) is characterized in terms of actuation and performance. (a) Actuation voltage: Dependence of the transmission polarization on voltage. Experimental data and corresponding polynomial fit are plotted for both liquid crystal retarders (black for LCA and red for LCB). Inset: experimental setup for characterization. PM: power meter, LP: linear polarizer, FG: function generator. (b) Performance: (Left) Transmitted light intensity with different polarization angles (black dots) shows excellent match to Malus's law (black line).  $\alpha$  is the angle between the transmission axes of the VTP and the linear polarizer. (Right) Uniform transmission over a broad input power range (50  $\mu$ W to 16 mW). Red line, 0° polarization; orange line, 30° polarization; cyan line, 60° polarization; purple line, 90° polarization.

After characterization, we then demonstrated the high-speed tuning of the transmission polarization using the VTP. By applying amplitude-modulated voltages to the liquid crystal retarders automatically, we were able to tune the transmission polarization of the VTP with a response time at the ms level. Figure 5(a) shows the high-speed periodic rotation of transmission polarization of the VTP under amplitude-modulated voltages. For each period, the actuation voltage was composed of 19 discrete levels where each level lasted 200 ms (Figure 5(a) bottom). The corresponding polarization directions were tuned from 0° to 90° and back to 0° in 10° increments. The transmitted light intensity was simultaneously recorded by an oscilloscope (Figure 5(a) black dots), fitting well to a sinusoidal function (Figure 5(a) red line) and indicating that the VTP responded well to dynamic actuation voltages. Also, no obvious fluctuation in the device performance was observed over multiple periods, showing great potential for long-term imaging applications. It should be mentioned that the transmission polarization tuning speed could be further improved at the cost of extinction ratio. For reference, Figure 5(b) shows the dependence of the extinction ratio on the time period of each voltage signal, reflecting the trade-off relation between the performance and the tuning speed. At a time period of 200 ms (or greater), the VTP exhibited a high extinction ratio (~250). However, we have observed the VTP can be still operated at a faster time period up to 50 ms at the expense of a lower extinction ratio of ~25.

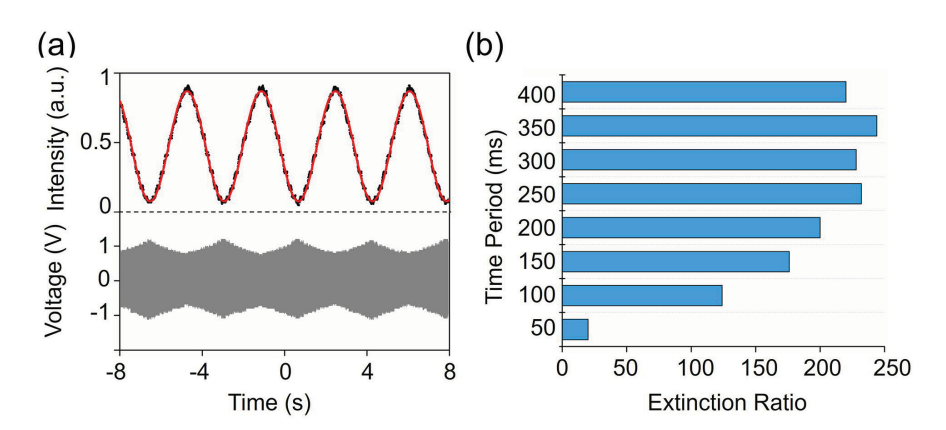


Figure 5. Voltage-tunable polarizer enables high-speed tuning of the transmission polarization. (a) Temporal performance: Top graph, transmitted light intensity of multiple periods under dynamic actuation (black dots, experimental data; red line, sinusoidal fit). Bottom graph, actuation voltages for operating the LCA, which is composed of 19 discrete voltage levels corresponding to tuning transmission axis from 0° to 90° and back to 0°. (b) Trade-off relation between the time period (i.e., tuning speed) and the extinction ratio: The experimental data are plotted as blue bars.

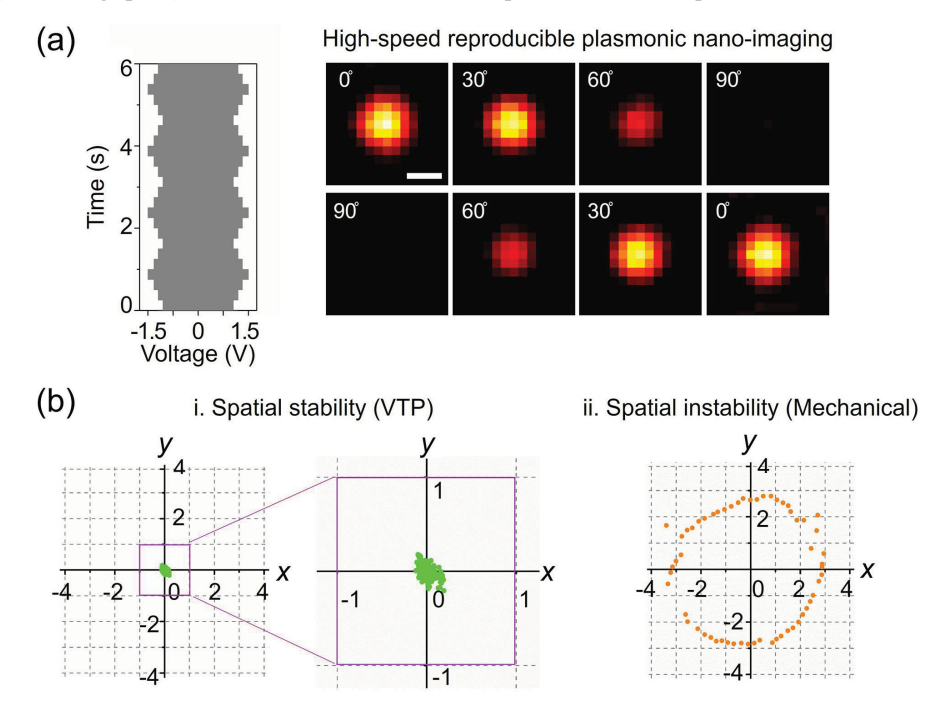


Figure 6. Voltage-tunable polarizer enables high-speed reproducible plasmonic nano-imaging with sub-pixel spatial stability. (a) High-speed reproducible plasmonic nano-imaging: Left graph, actuation voltages for high-speed imaging. Right graph, reproducible nanorod dark-field images with transmission polarization from 0° to 90° and back to 0°. The scale bar is 1 µm. (b) Quantitative measurement of spatial stability: (i) Scatter plots were constructed from the beam center on every image (green dots), revealing sub-pixel spatial stability. x and y coordinates represent the spatial position in pixel units. (ii) Scatter plots of the unstable images arise from a mechanical rotated polarizer (orange dots). x and y coordinates represent the spatial position in pixel units. The centroid algorithm uses least squares 2D Gaussian fitting approach to determine the beam center in images. At the polarization angles close to 90° (perpendicular to the nanorod orientation), the intensity of the nanorod decreased to almost zero, making the centroids in those images difficult to determine using algorithms. Therefore, the centroids at those images were excluded and not plotted in the figure.

Finally, high-speed reproducible plasmonic nano-imaging with spatial stability beyond the pixel limit is illustrated in Figure 6. Polarimetric images of a single nanorod were taken automatically with a polarization transition time of 250 ms. The voltage control (Figure 6(a) left) and the image acquired from the CCD were automated to realize high-speed

imaging with a 50-ms integration time. As shown in the selected representative images (Figure 6(a) right), the nanorod maintains its absolute position without introducing any significant beam deviation errors under high-speed polarization tuning. For quantitative analysis, the beam center on every image was determined by a Gaussian fit centroiding algorithm using MATLAB (Figure 6(b)-i). The images were acquired from a standard, mechanical setup (using a mechanical polarizer to rotate the polarization) and tracked for reference (Figure 6(b)-ii). As shown, unlike the mechanical setup, in which the beam deviation is as large as  $\sim \pm 3$  pixels, our system is able to offer spatially stable polarimetric images with beam deviations smaller than  $\pm 0.21$  pixels throughout the high-speed tuning of the transmission polarization. Such a capability is vital in real-time super-resolution applications (*e.g.*, intracellular bio-imaging) where sub-pixel precision and high time resolution are desired.

#### 5. CONCLUSION

In summary, we have demonstrated a spatially stable polarimetric nano-imaging system, consisting of our voltage-tunable polarizer integrated into an optical microscope (dark-field), for high-speed plasmonic bio-imaging. Voltage, rather than mechanical rotation, was applied to tune the polarization transmission axis with a fast response time (ms). Compared to conventional setups, our system can provide spatially stable (sub-pixel level) and high-speed imaging with excellent repeatability. We expect that our system should allow for real-time acquisition of accurate spatial information in bio-plasmonic imaging applications where high precision and time resolution are required.

#### 6. ACKNOWLEDGEMENTS

This work was supported by the National Science Foundation (NSF) and the Air Force Office of Scientific Research (AFOSR).

#### REFERENCES

- [1] Sönnichsen, C. and Alivisatos, A. P., "Gold nanorods as novel nonbleaching plasmon-based orientation sensors for polarized single-particle microscopy," Nano Lett. **5**(2), 301–304 (2005).
- [2] Chang, W.-S., Ha, J. W., Slaughter, L. S., and Link, S., "Plasmonic nanorod absorbers as orientation sensors," Proc. Natl. Acad. Sci. U. S. A. 107(7), 2781–2786 (2010).
- [3] Wang, H. F., Huff, T. B., Zweifel, D. A., He, W., Low, P. S., Wei, A., and Cheng, J.-X., "In vitro and in vivo two-photon luminescence imaging of single gold nanorods," Proc. Natl. Acad. Sci. U. S. A. 102(44), 15752–15756 (2005).
- [4] Ming, T., Zhao, L., Yang, Z., Chen, H., Sun, L., Wang, J., and Yan, C., "Strong polarization dependence of plasmon-enhanced fluorescence on single gold nanorods," Nano Lett. 9(11), 3896–3903 (2009).
- [5] Wang, G., Sun, W., Luo, Y., and Fang, N., "Resolving rotational motions of nano-objects in engineered environments and live cells with gold nanorods and differential interference contrast microscopy," J. Am. Chem. Soc. **132**(46), 16417–16422 (2010).
- [6] Olson, J., Dominguez-Medina, S., Hoggard, A., Wang, L.-Y., Chang, W.-S., and Link, S., "Optical characterization of single plasmonic nanoparticles," Chem. Soc. Rev. 44(1), 40–57 (2015).
- [7] Wang, P., Zhang, L., Xia, Y., Tong, L., Xu, X., and Ying, Y., "Polymer nanofibers embedded with aligned gold nanorods: a new platform for plasmonic studies and optical sensing," Nano Lett. **12**(6), 3145–3150 (2012).
- [8] Ringe, E., Sharma, B., Henry, A.-I., Marks, L. D., and Van Duyne, R. P., "Single nanoparticle plasmonics," Phys. Chem. Chem. Phys. 15(12), 4110–4129 (2013).
- [9] Azzam, R. M. A., "Stokes-vector and Mueller-matrix polarimetry," J. Opt. Soc. Am. A 33(7), 1396–1408 (2016).
- [10] Kavaldjiev, D. and Ninkov, Z., "Influence of nonuniform charge-coupled device pixel response on aperture photometry," Opt. Eng. **40**(2), 162–169 (2001).